Synthesis and Crystallization Behavior of Acetal Copolymer/Silica Nanocomposite by *In Situ* Cationic Ring-Opening Copolymerization of Trioxane and 1,3-Dioxolane

Lanhui Sun,[1] Zhen-Guo Yang,[1] Xiaohui Li[2]

[1]*Department of Materials Science, Fudan University, Shanghai 200433, People's Republic of China*
[2]*Shanghai Research Institute of Materials, Shanghai 200437, People's Republic of China*

Received 13 July 2007; accepted 17 August 2007
DOI 10.1002/app.27258
Published online 25 October 2007 in Wiley InterScience (www.interscience.wiley.com).

ABSTRACT: The acetal copolymer/silica nanocomposite was prepared by *in situ* bulk cationic copolymerization of trioxane and 1,3-dioxolane in the presence of nanosilica. The crystallization behavior of acetal copolymer/silica nanocomposite was studied by AFM, DSC, XRD, and CPOM, and the macromolecular structure of acetal copolymer/silica nanocomposite was characterized by FTIR and ^{1}H-NMR. The ^{1}H-NMR results showed that the macromolecular chain of acetal copolymer had more than two consecutive 1,3-dioxolane units in an oxymethylene main chain, while that of acetal copolymer/silica nanocomposite had only one 1,3-dioxolane unit in an oxymethylene main chain. There existed interaction between the macromolecular chains and nanoparticles (such as hydrogen bonds and coordination). On one hand, nanoparticles acted as nucleation center, which accelerated the crystallization rate but reduced the crystallinity. The spherulite sizes also decreased with addition of nanoparticles attributed to the nucleation effect. On the other hand, the presence of nanoparticles interrupted the spherical symmetry of the crystallite. In conclusion, the high surface energy and small scale of nanoparticles have a prominent impact on the polymerization mechanism and crystallization behavior of nanocomposite. © 2007 Wiley Periodicals, Inc. J Appl Polym Sci 107: 1842–1849, 2008

Key words: acetal copolymer; crystallization behavior; *in situ* polymerization; nanocomposites

INTRODUCTION

Acetal resin has linear macromolecular consisting of CH_2O structural units, which can be prepared from formaldehyde or from its cyclic oligomers, such as trioxane by homopolymerization or copolymerization. The copolymerization of trioxane is of considerable industrial importance, because the copolymer has better thermal properties and superior resistance to alkali than homopolymer. This is because the degradation of the copolymer by successive removal of formaldehyde stops when the sequence of CH_2O units is interrupted by a C—C bond in copolymer.[1] But acetal copolymer has reduced crystallinity as a result of C—C units interspersed in its polymer chain, which interrupts the regularity of polymer chain.

Acetal copolymer resin is typically prepared by the cationic ring-opening copolymerization of trioxane and a cyclic ether, such as ethylene oxide[2–9] or 1,3-dioxolane.[10–13] The copolymerization can be initiated by Lewis acid such as $BF_3 \cdot O(Et)_2$, $TiCl_4$[14] and $CH_3CO ClO_4$[15] as well as $MoO_2(C_5H_7O_2)_2$.[11] $BF_3 \cdot O(Et)_2$ and $BF_3 \cdot O(Bu)_2$ are usually used as the catalyst for the commercial production of acetal copolymer. According to the results obtained so far, no termination takes place in the polymerization unless terminator is added. To terminate the polymerization, triethylamine or acetic anhydride should be used.

Collins et al. believed that during the copolymerization of ethylene oxide and trioxane, ethylene oxide was converted to 1,3-dioxolane, 1,3,5-trioxepane (TOXP), and to low-molecular weight linear copolymer. They stated that because of the weak basicity of trioxane, a direct reaction of trioxane and ethylene oxide was impossible.[2] Although the ethylene oxide was consumed during the initial stage of the reaction, the ethylene oxide monomer unit distribution in the final polymer could be close to that of a random copolymer.[16]

However, there is a newly discovered mechanism for the copolymerization of trioxane and ethylene oxide: several new intermediates are found, including 1,3,7-tetraoxacyclononane (TOCN), 1,3,5,7,10-pentaoxacyclododecane (POCD), and 1,3,5,7,10,13-hexaoxacycloheptadecane (HOCP), which are the products

Correspondence to: Z.-G. Yang (zgyang@fudan.edu.cn).
Contract grant sponsor: Shanghai Science and Technology Development Foundation; contract grant number: 06DZ22012.

Journal of Applied Polymer Science, Vol. 107, 1842–1849 (2008)
© 2007 Wiley Periodicals, Inc.

from the direct reaction of trioxane and ethylene oxide.[17,18] All these intermediates transfer to 1,3-dioxolane and TOXP in the latter period of the polymerization. This might be attributed to the higher ring strain energy of the high-numbered ring compound of TOCN, POCN, and HOCP compared with those of the low-numbered ring compounds such as 1,3-trioxane and TOXP. The copolymer from trioxane and ethylene oxide will give a polymer with one, two, or three consecutive oxyethylene units in an oxymethylene main-chain sequence dependant on the ratio of trioxane and ethylene oxide.

When 1,3-dioxolane is substituted for ethylene oxide, a small induction period is observed. Yamasaki et al.[16] pointed out that the copolymerization of 1,3-dioxolane with trioxane would give only one oxyethylene sequence in an oxymethylene main chain, which was different from the consecutive oxyethylene sequences in copolymer of trioxane and ethylene oxide.

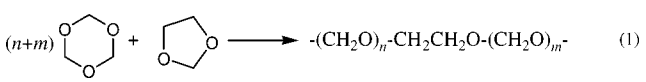

(1)

The crystallization during polymerization of trioxane has been extensively studied.[8,19–23] The polymerization of trioxane is a typical example of simultaneous polymerization and crystallization, since the polymer is insoluble and crystallizes at a high rate in conventional solvents during cationic polymerization. According to Kohlschutter and Sprenger,[19,20] this polymerization took place on the surface of the trioxane crystals. Matsuzaki et al.[8] found that large spherulites were deduced from the clear and strong growth of the lamellae. They assumed that a fibril structure having extended chain-like crystals or highly regular crystals, which were created by the crystallization during polymerization. The molecular chain of this crystal was thought to be regularly arrayed and thus overall less entangled. Less polymer chain entanglement was thought to cause fewer nucleation sites for crystallization, thus forming the large spherulites and strong growth of lamellae.

In situ polymerization is an effective method for the preparation of inorganic-polymeric nanocomposite.[24–27] Nanoscale inorganic fillers have good dispersibility, since monomers have good motility due to their small sizes before the polymerization, thus they can penetrate through the agglomerated nanoscale inorganic fillers. Then the monomers are polymerized *in situ*, which depresses the agglomeration of nanoscale inorganic fillers. A lot of nanocomposites have been prepared by *in situ* polymerization such as PE/Al_2O_3,[28] PA6/MMT,[29] PP/silica,[30] and so on. The mechanical properties,[28–31] thermal stability,[31] glass transition temperature, and crystallization behavior[32] have been improved.

The crystallization behavior of inorganic-polymeric nanocomposite in the presence of inorganic filler has been extensively studied.[33–39] However, the characteristic crystallization behavior of nanocomposite due to the large specific surface area of nanoparticles has not been well understood. Usually the addition of nanoparticles results in the heterogeneous nucleation effect. It has been reported that the addition of $CaCO_3$ increased the crystallization rate of PP and decreased the spherulite size attributed to the heterogeneous nucleation effect of $CaCO_3$.[33,34] Zheng et al.[38] pointed out that ZnO nanoparticles had two competing effects on the crystallization of nylon-6: inducing the nucleation but retarding the mobility of polymer chains. Zheng et al.[39] reported that nanosilica did not behave as nucleation agent in PET but postponed the appearance of crystallite.

However, there is few investigation on *in situ* cationic ring-opening copolymerization of acetal copolymer/silica nanocomposite. Also, the crystallization behavior of acetal copolymer in the presence of nanosilica has rarely been reported, especially when the nanocomposite is prepared by *in situ* polymerization. In this article, we studied the effect of nanoparticles on the polymerization mechanism and crystallization behavior of nanocomposite. Bulk polymerization of trioxane and 1,3-dioxolane was carried out using $BF_3 \cdot O(Et)_2$ as catalyst in the presence of nanosilica. The morphology of acetal copolymer/silica nanocomposite was observed on field emission scanning electron microscope (FESEM) and atomic force microscopy (AFM). Fourier transform infrared (FTIR) spectroscopy and ^{1}H-NMR spectrometry were used for the determination of copolymer sequences. We also studied the crystallization behavior of acetal copolymer in the presence of nanosilica using differential scanning calorimetry (DSC) and X-ray diffraction (XRD) as well as cross-polarization optical microscopy (CPOM). We focused on the effect of the inorganic filler on the crystallization behavior of acetal copolymer, especially on the crystallinity, crystal size, and morphology.

EXPERIMENTAL

Materials

Trioxane was purchased from Shanghai Shengyu Chem (China). It was dried in vacuum for 24 h at 90°C to eliminate moisture and methanol. The average particle size of nanosilica was below 35 nm as reported by the manufacturer, Hehai Nanophase Technologies Corporation, Jiangsu Province of China. Nanosilica was treated with silane coupling agent KH-550 before polymerization with the intention of increasing the compatibility between organic–inorganic phases. 1,3-Dioxolane was supplied by Johnson Matthey, which was immersed in zeolite and purified by the elimination

of water. $BF_3 \cdot O(Et)_2$ was obtained from Sinopharm Group Chemical Reagent (China). Triethylamine and methanol were both commercially available.

Nanocomposite preparation

Nanocomposite was prepared by using *in situ* polymerization, where a bulk polymerization similar to the method for the industrial production of the acetal copolymer from trioxane and 1,3-dioxolane was applied. Purified trioxane was melted in a flask immersed in an oil bath at 70°C. 1,3-Dioxolane (4.5 mol % to trioxane) and nanosilica (1 wt % to trioxane) were introduced into the molten trioxane. $BF_3 \cdot O(Et)_2$ catalyst (5×10^{-4} mol % to trioxane) was injected into the mixture with a syringe. The system was stirred with a mixer during the polymerization. The powdery reaction product was poured into a methanol solution, which contained 0.5 wt % triethylamine to deactivate the catalyst, and then was washed with methanol several times, and dried in vacuum for further characterization.

Characterization

FESEM was carried out in a Philips XL30 FESEM. Before experiment, the sample was ion plated with Au to become conductive. AFM images of the nanocomposite were recorded by a SPA-300HV (Seiko Instrument) in tapping mode with a silica probe. The sample was prepared by casting molten acetal copolymer/silica nanocomposite onto clear glass substrates with surface roughness (Ra) below 2 μm and dried at room temperature before AFM observation. The mixture of powdery product and KBr (100–200 times to powdery product) was ground to below 2.5 μm, and pressed to thin film, which was analyzed by a Peakin Elmer PARAGON 10,001 FTIR spectroscopy. ^{1}H-nuclear magnetic resonance (^{1}H-NMR) spectra was recorded with JNM-MY60FT spectrometer in $CDCl_3$, and the chemical shifts (δ) in ppm were referenced to internal tetraethylsilane. DSC analysis was conducted on a Peakin Elmer DSC-6 at a heating rate of 10°C/min from 50 to 300°C in nitrogen atmosphere. XRD study was carried out on a D/max-γB X-ray diffractometer at a scanning rate of 6 deg/min. CPOM was carried out in an Olympus BH-2 optical microscope, equipped with a digital camera.

RESULTS AND DISCUSSION

Morphology

Figure 1 shows the morphology of acetal copolymer/silica nanocomposite and nanoparticles dispersion in acetal copolymer matrix. Absence of voids or gaps between nanoparticles and acetal copolymer matrix indicates good compatibility between organic–inorganic phases. Nanoparticles are well wrapped by acetal copolymer matrix and have good dispersibility. The average diameter of nanoparticles is about 100 nm, which indicates that every nanoparticle contains 2–3 nanosilica. Usually primary nanaopartiles tend to form secondary nanoparticles in polymer matrix. It is suggested that monomers can penetrate through the agglomerated nanoparticles because of their small sizes before the polymerization. Once the initiator is added to the system the monomers are polymerized *in situ*, and the growing macromolecular chains in the vicinity of nanoparticles separate the nanoparticles from agglomeration during *in situ* polymerization.

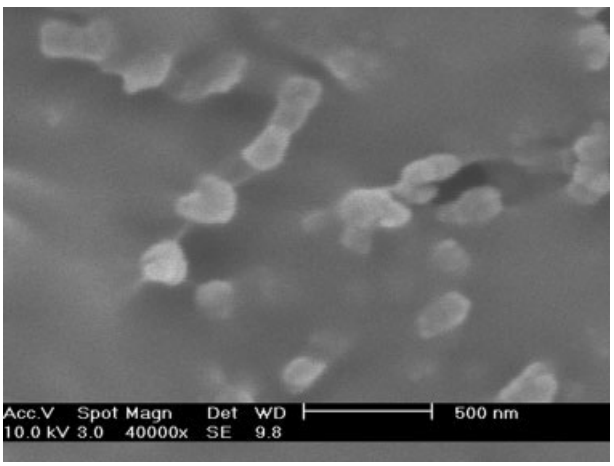

Figure 1 FESEM image of acetal copolymer/silica nanocomposite.

AFM images at low magnification [Fig. 2(a,b)] provide evidence for the homogeneous dispersion of nanoparticles in acetal copolymer matrix. It is clearly seen in AFM images of acetal copolymer/silica nanocomposite at high magnification [Fig. 2(c,d)] that the approximate dimension of nanoparticles is 100 nm in diameter. AFM phase images [Fig. 2(b,d)] reveal a series of dark and light spots. Because AFM phase images can detect variations in composition, adhesion, friction, and viscoelasticity (stiffness, modulus), this result indicates that there exist two phases in nanocomposite: softer organic phase (lighter region) and stiffer inorganic phase (darker region). Curved individual lamellae or lamellar bundles are observed from Figure 2(b). The lamellar thickness is about 20 nm. Nanoparticles are wrapped in the crystallite, Figure 2(d). Some nanoparticles which act as nucleation agent may absorb some monomers on the surface because of high surface energy. Since the polymerization of trioxane is a typical example of simultaneous polymerization and crystallization, once the nucleation happens at the surface of nanoparticles,

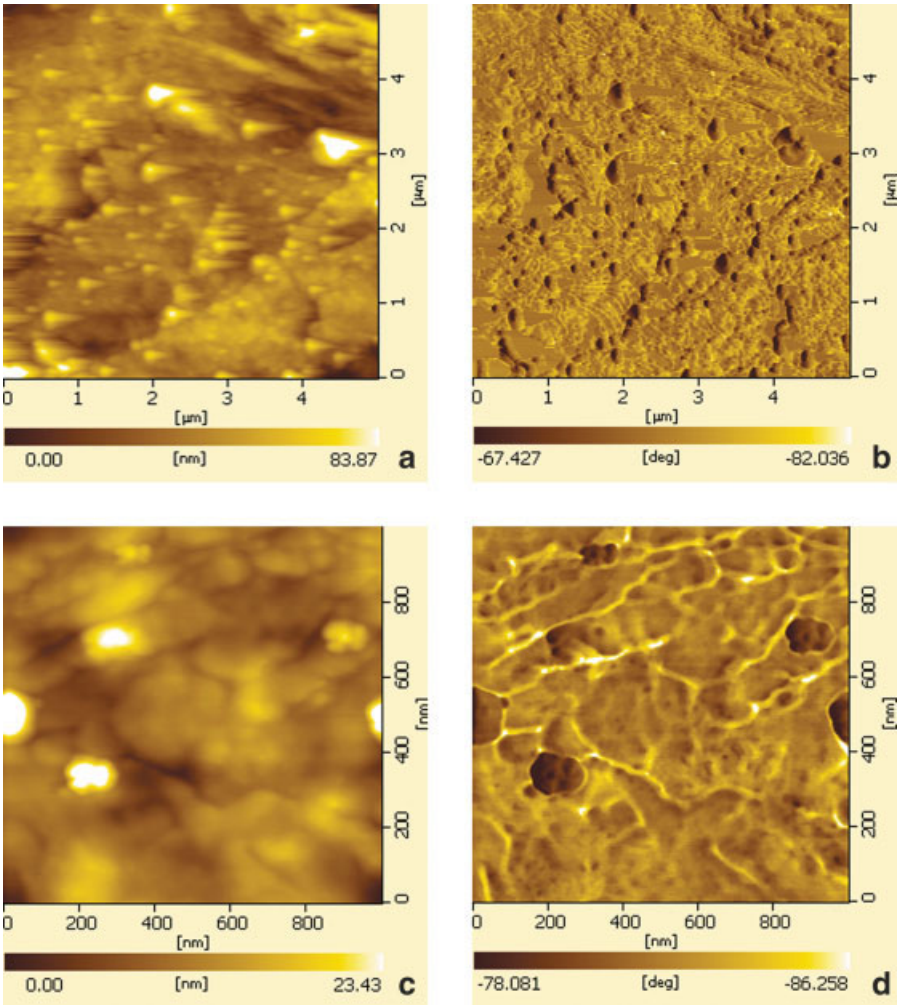

Figure 2 AFM images of acetal copolymer/silica nanocomposite: (a) height mode at low magnification, (b) phase mode at low magnification (c) height mode at high magnification, and (d) phase mode at high magnification. [Color figure can be viewed in the online issue, which is available at www.interscience.wiley.com.]

lamellae grow quite successively around nanoparticles through direct addition of the monomer molecules onto the reactive chain ends. Thus the secondary nucleation mechanism leads to the acceleration of nucleation compared to that without the addition of nanoparticles, which will be discussed later.

Structural characterization of acetal copolymer/silica nanocomposite

Figure 3 shows the FTIR spectra of acetal copolymer/silica nanocomposite and acetal copolymer from copolymerization of trioxane and 1,3-dioxolane. They both show strong characteristic peaks of acetal copolymer at 1239 and 1093 cm^{-1}. The absorption bands at 900, 935, and 1239 cm^{-1} are due to the symmetric stretching vibration of C—O—C and the rocking vibration of $—CH_2—$. The absorption band at 1093 cm^{-1} results from asymmetric stretching vibration of C—O—C and bending vibration of O—C—O. The double peaks of stretching vibration of C—C are also found at 2983 and 2923 cm^{-1}. The absorption peak at 1470 cm^{-1} is due to bending vibration of C—C. Comparing the FTIR spectra of acetal copolymer/silica nanocomposite with acetal copolymer, we can see that the infrared absorption band of C—O—C at 1093 cm^{-1} is broadened because of the asymmetric stretching vibration of Si—O—Si. The FTIR spectra of acetal copolymer/silica nanocomposite has an additional absorption peak at 976 cm^{-1} compared to that of acetal copolymer, which is due to the association (such as hydrogen bonds and coordination) between the high-energy active sites on the surface of nanosilica and the macromolecular chains of acetal copolymer. This suggests that nanoparticles are well included in the synthesized product (acetal copolymer/silica nanocomposite). The existence of the only two weak bands characteristic of silica may be due to the low content of silica in the acetal copolymer/silica nano-

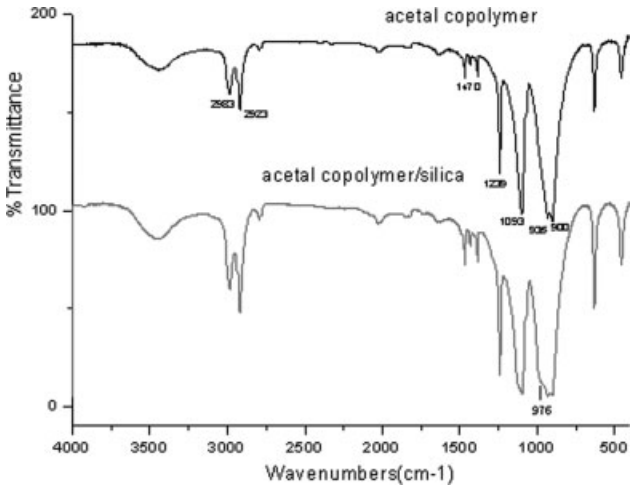

Figure 3 FTIR spectra of acetal copolymer and acetal copolymer/silica nanocomposite.

composite. But there is no evidence of chemical interaction between the organic–inorganic phases.

The ^{1}H-NMR spectra of the oxymethylene unit (—CH_2O—) and oxyethylene unit (—CH_2CH_2O—) of acetal copolymer and acetal copolymer/silica nanocomposite are shown in Figure 4. The methylene proton signal Ha of the oxymethylene unit is observed at 4.84–4.99 ppm, which is split into three signals corresponds to copolymer MMM sequence. The signal resulting from the 1,3-dioxolane monomer is divided into three signals: Hb_1 at 3.70–3.85 ppm, Hb_2 at 4.082 ppm, and Hb_3 at 4.285 ppm. Signal Hb_1 and Hb_2 can be assigned to oxyethylene unit, and Hb_3 can be assigned to the methylene proton of oxymethylene unit located between two consecutive oxyethylene units. These three signals indicate that the macromolecular chain of acetal copolymer has more than two consecutive 1,3-dioxolane structural units in an oxymethylene main chain. This result differs from the result of Yamasaki's: the copolymerization of 1,3-dioxolane with trioxane will give only one oxyethylene sequence in an oxymethylene main chain.[16] The mechanism may be explained as follows, during the chain propagation period the increasing chain attacks two or more 1,3-dioxolane consecutively as shown below

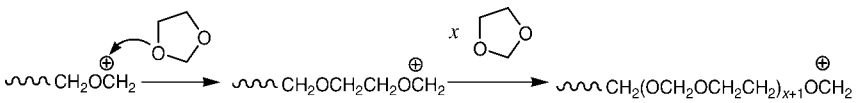

(2)

For the ^{1}H-NMR spectra of acetal copolymer/silica nanocomposite, the signals of oxymethylene unit (appear at 4.84–4.99 ppm) remain almost the same compared to that of acetal copolymer. However, only ethylene proton signal Hb_1 can be observed at 3.70–3.85 ppm, which is in good accordance with that of acetal copolymer. Surprisingly the ethylene proton signal Hb_2 and Hb_3 disappear in acetal copolymer/silica nanocomposite, which means there is only one 1,3-dioxolane unit in an oxymethylene main chain. This may be explained as follows, during the chain propagation period the increasing chain only attacks one 1,3-dioxolane consecutively as shown below

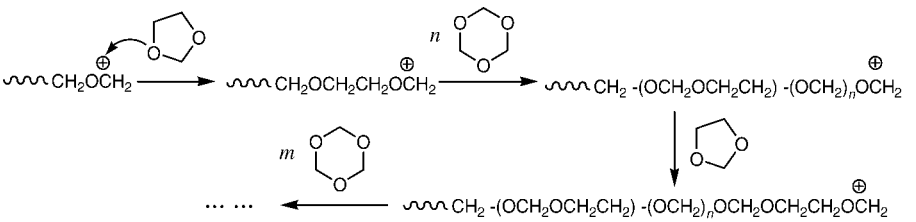

(3)

The reason has not been well understood, but we suppose that during the chain propagation period the active sites on the surface of nanosilica can ''absorb'' some 1,3-dioxolane monomers. As a result this gives only one 1,3-dioxolane unit in an oxymethylene main chain. Furthermore there appears a signal at 5.163 ppm, which is because the interaction between the macromolecular chains and the active sites on the surface of nanosilica (such as hydrogen bonds and coordination), which has a deshielding effect on the oxymethylene proton. Here nanosilica act as electron donor due to the lone pairs of electrons on the surface, and oxymethylene units act as electron acceptor. Thus, δ shifts to low field. FTIR analysis also proves the interaction between the copolymer chain and nanosilica.

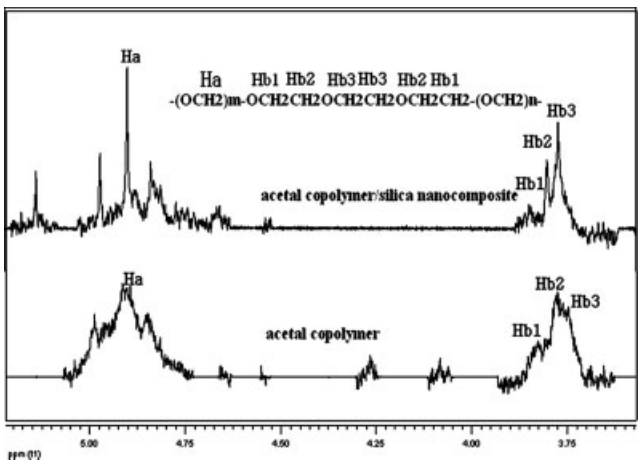

Figure 4 ^{1}H-NMR spectra of acetal copolymer and acetal copolymer/silicananocomposite.

Crystallization behavior of acetal copolymer/silica nanocomposite

The DSC heating curve of acetal copolymer/silica nanocomposite is shown in Figure 5, from which we can get the melting peak temperature (t_p) and melting enthalpy (ΔH), thus crystallinity (Xc) can be calculated. We can also make qualitative analysis on crystallization rate. A summary of the DSC data which corresponds to the curve is shown in Table I. It can be seen from Table I that the crystallinity of acetal copolymer/silica nanocomposite decreases compared to neat acetal copolymer. ($t_{onset} - t_p$) reflects the overall crystallization rate, the smaller it is the rapider is the crystallization rate. So the crystallization rate of acetal copolymer is accelerated with the addition of nanoparticles. It is suggested that nanoparticles exhibit strong nucleation effects, which can be attributed to reducing the specific surface free energy for nuclei formation during crystallization and consequently the increase of the crystallization rate.

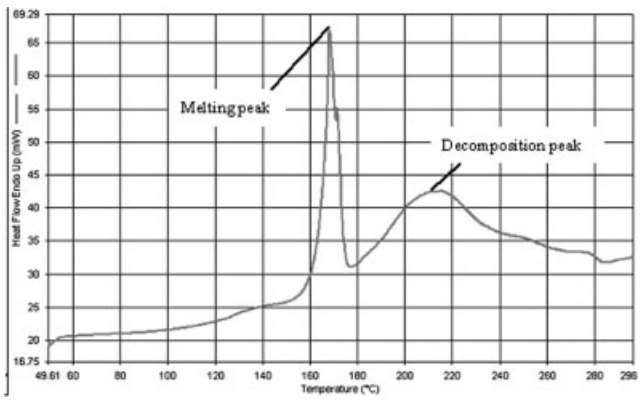

Figure 5 DSC curve of acetal copolymer/silica nanocomposite.

TABLE I
DSC Data of Acetal Copolymer/Silica Nanocomposite and Acetal Copolymer

Sample	t_{onset} (°C)[a]	t_p (°C)[b]	($t_{onset} - t_p$) (°C)	ΔH (J/g)	Xc (%)
Acetal copolymer/silica	165.4	168.33	2.928	164.953	67.19
Acetal copolymer[c]	156.3	166.81	10.416	202.277	81.56

[a] t_{onset}: onset temperature of melting.
[b] t_p: peak temperature of melting.
[c] Acetal copolymer: Commercially available M60- acetal copolymer produced by Formosa Plastics Corporations Limited.

XRD spectra of acetal copolymer and acetal copolymer/silica nanocomposite are shown in Figure 6, from which we can see that both acetal copolymer and acetal copolymer/silica nanocomposite show strong and sharp diffraction peak. The amorphous regions appear as a broad halo under the strong and sharp diffraction pattern of the crystallites. Diffraction from the (100), (105), and (110) planes in acetal copolymer/silica nanocomposite are centered at 22.900°, 34.520°, and 48.240°, the values are close to the 22.760°, 34.380°, and 48.120° of neat acetal copolymer. This indicates that the addition of nanoparticles does not alter or distort the crystal structure of acetal copolymer, which is a hexagonal structure. On the other hand, the widths of the diffraction peaks of acetal copolymer/silica nanocomposite are broader than that of neat acetal copolymer. The peak width is related to the internal strain, crystallite size, and degree of perfection of the crystallites. Given that the peaks are broadened, we can assume that there is internal strain in acetal copolymer/silica nanocomposite. The interplanar distances and crystallite sizes,

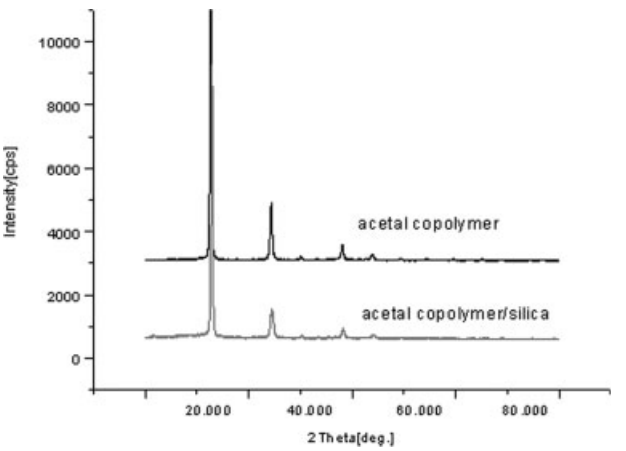

Figure 6 XRD spectra of acetal copolymer and acetal copolymer/silica nanocomposite.

TABLE II
Crystallite Sizes of Acetal Copolymer and Acetal Copolymer/Silica Nanocomposite

	Interplanar distance (Å)			Lamellar thickness (nm)		
Sample	L_{100}	L_{105}	L_{110}	L_{100}	L_{105}	L_{110}
Acetal copolymer	3.9038	2.6063	1.8894	26.51	16.85	18.49
Acetal copolymer/silica	3.8803	2.5961	1.8849	24.66	14.74	18.50

calculated from the Dbye-Sherrer method, are shown in Table II. The results indicate that the addition of nanoparticles has little effect on the interplanar distance of acetal copolymer. However, lamellar thicknesses of acetal copolymer at (100) and (105) planes decrease, which is due to the heterogeneous nucleation of acetal copolymer at the presence of nanoparticles. But at (110) plane lamellar thickness remains almost the same. The lamellar thicknesses vary in the range of 10–30 nm, which can be proven by AFM phase image [Fig. 2(b)]. The crystallization rate is also accelerated resulting from the nucleation effect of nanoparticles. This is supported by the DSC results mentioned earlier.

CPOM is used to compare the crystal morphology between filled and unfilled acetal copolymer synthesized from copolymerization of trioxane and 1,3-dioxolane, which are both crystallized at 50°C. For neat acetal copolymer, it can be seen from Figure 7(a) that the spherulites are similar in size. For acetal copolymer/silica nanocomposite [Fig. 7(b,c)] the spherulites have inhomogeneous sizes and they are smaller than those of neat acetal copolymer. We can see from Figure 7(c) that some nanoparticles reside in the spherulites of acetal copolymer/silica nanocomposite. It is suggested that when the growing lamellae encounter nanoparticles, the lamellar pathways are interrupted and they are forced to grow around the nanoparticles, breaking the spherical symmetry of the crystallite. Therefore the effect of nanoparticles on the crystallite growth results in spherulites grown in a haphazard fashion with tortuous lamellar pathways.

CONCLUSIONS

Acetal copolymer/silica nanocomposite were successfully synthesized by cationic ring-opening *in situ* polymerization of trioxane and 1,3-dioxolane. Nanoparticles had good dispersibility in acetal copolymer matrix, and the average size was about 100 nm. Nanoparticles were wrapped in the crystallite, which not only acted as nucleation center but also interrupted the spherical symmetry of the crystallite. Thus the crystallization rate was accelerated significantly, while the crystallinity of acetal copolymer/silica nanocomposite decreased because of the heterogeneous nucleation. The results of CPOM indicated that the spherulite sizes decreased with the addition of nanoparticles, and the presence of nanoparticles resulted in spherulites grown in a haphazard fashion with tortuous lamellar pathways.

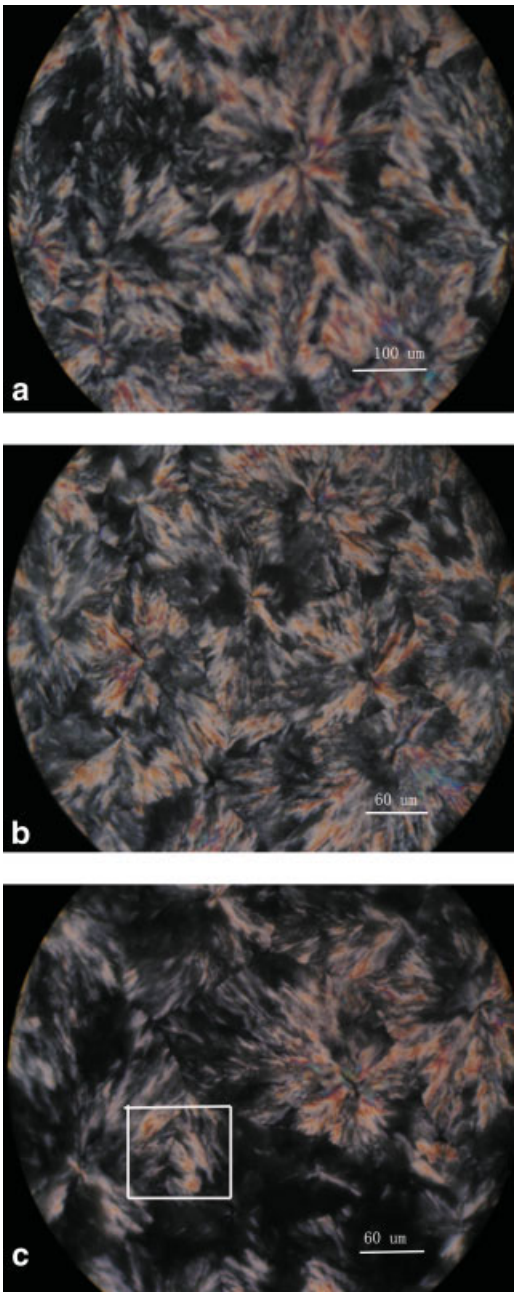

Figure 7 CPOM images of neat acetal copolymer and acetal copolymer/silica nanocomposite: (a) neat acetal copolymer, (b) acetal copolymer/silica nanocomposite, and (c) acetal copolymer/silica nanocomposite. [Color figure can be viewed in the online issue, which is available at www.interscience.wiley.com.]

The results of FTIR and ^{1}H-NMR indicated that the *in situ* polymerization product was acetal copolymer. ^{1}H-NMR results showed that there existed two or more consecutive 1,3-dioxolane units in an oxymethylene main-chain sequence polymerized from trioxane and 1,3-dioxolane, which differed from the previous results of Yamasaki. However, the macromolecular chain of acetal copolymer/silica nanocomposite had only one 1,3-dioxolane in an oxymethylene main chain. This was due to the active sites on the surface of nanoparticles ''absorbed'' some 1,3-dioxolane monomers during the chain propagation period.

References

1. Wissermel, K.; Fischer, E.; Gutweiler, K.; Hermann, H. D.; Chedon, H. Angew Chem Int Ed Engl 1967, 6, 526.
2. Collins, G. L.; Greene, R. K.; Beeradinelle, F. M.; Ray, W. H. J Polym Sci Polym Chem Ed 1981, 19, 1597.
3. Yamasaki, N.; Masamoto, J.; Kanaori, K. Appl Spectrosc 2000, 54, 1069.
4. Chen, C. S. H.; DiEdwardo, A. Adv Chem Ser 1969, 91, 359.
5. Chen, C. S. H.; DiEdwardo, A. J Macromol Sci A 1970, 4, 349.
6. Jaacks, V. Makromol Chem 1967, 101, 33.
7. Yamasaki, N.; Kanaori, K.; Masamoto, J. J Polym Sci Part A: Polym Chem 2001, 39, 3239.
8. Matsuzaki, K.; Maeda, M.; Kondo, M.; Morishita, H.; Hamada, M.; Yamaguchi, T.; Neki, K.; Masamoto, J. J Polym Sci Part A: Polym Chem 1997, 35, 2479.
9. Yamasaki, N.; Masamoto, J. J Polym Sci Part A: Polym Chem 2004, 42, 520.
10. Shieh, Y. T.; Lay, M. L.; Chen, S. A. J Polym Res 2003, 10, 151.
11. Chen, C. S. H.; Wenger, F. J Polym Sci Part A: Polym Chem 1971, 9, 33.
12. Sextro, G.; Burg, K.; Cherdron, H. Makromol Chem 1976, 177, 1815.
13. Burg, K. H.; Leugering, H.; Sextro, G Angew Chem 1974, 13, 418.
14. Bell, R. P.; Skinner, B. G. J Chem Soc [London] 1952, 2955.
15. Kern, W.; Jaacks, V. J Polym Sci 1960, 48, 399.
16. Yamasaki, N.; Masamoto, J.; Kanaori, K. J Appl Spectrosc 2000, 54, 1069.
17. Yamasaki, N.; Naganara, H.; Masamoto, J. Tetrahedron Lett 2001, 42, 271.
18. Yamasaki, N.; Masamoto, J. Nippon Kagaku Kaishi 2001, 10, 371.
19. Jamison, Cf. S. E.; Noether, H. D. J Polym Sci Part B: Polym Lett 1963, 1, 51.
20. Kohlschutter, H. W.; Sprenger, L. Z Physik Chem 1932, B16, 284.
21. Wegner, G.; Rodriguez-Baeza, M. Makromol Chem 1980, 181, 1763.
22. Mateva, R.; Wegner, G.; Lieser, G. J Polym Sci Polym Lett Ed 1973, 11, 369.
23. Iguchi, M.; Kanitsuna, H.; Kawai, T. Makromol Chem 1969, 128, 63.
24. Godovsky, D. Y. Adv Polym Sci 2000, 153, 163.
25. Ahmadi, S. J.; Huang, Y. D.; Li, W. J Mater Sci 2004, 39, 1919.
26. Rong, M. Z.; Zhang, M. Q.; Zheng, Y. X.; Zeng, H. M.; Walter, R.; Friedrich, K. J Mater Sci Lett 2000, 19, 1159.
27. Gilman, J. W.; Bourbigot, S.; Shields, J. R.; Nyden, M.; Kashiwagi, T.; Davis, R. D.; Vanderhart, D. L.; Demory, W.; Wilkie, C. A.; Morgan, A. B.; Harris, J.; Lyon, R. E. J Mater Sci 2003, 38, 4451.
28. Zhang, X.; Simon, L. C. Macromol Mater Eng 2005, 290, 573.
29. Kyu, T.; Zhou, Z. L.; Tajuddin, Y.; Qutubuddin, S. J Polym Sci Part B: Polym Phys 1996, 34, 1761.
30. Zhang, M. Q.; Rong, M. Z.; Zhang, Z. W. J Mater Sci 2004, 39, 3475.
31. Wu, R. D.; Tong, X. L.; Fei, Z. X. Polym Mater Sci Eng 2006, 22, 59.
32. Yang, F.; Ou, Y. C.; Yu, Z. J Appl Polym Sci 1998, 69, 355.
33. Lin, Z. D.; Huang, Z. Z. J Appl Polym Sci 2004, 91, 2443.
34. Khare, A.; Mitra, A.; Radhakrishnan, S. J Mater Sci 1996, 31, 5691.
35. Qian, J. S.; He, P. S.; Nie, K. M. J Appl Polym Sci 2004, 91, 1013.
36. Lu, D.; Mai, Y. W. Macromol Mater Eng 2003, 288, 693.
37. Xu, W.; Ge, M.; He, P. J Appl Polym Sci 2001, 82, 2281.
38. Zheng, J. R.; Siegel, R. W.; Toney, G. J Polym Sci Part B: Polym Phys 2003, 41, 1033.
39. Zheng, H.; Wu, J. L. J Appl Polym Sci 2007, 103, 2564.